

Simulation of chiral motion of excitation within the ground-state manifolds of neutral atoms

Hao-Yuan Tang,¹ Xiao-Xuan Li,² Jia-Bin You,^{3, a)} and Xiao-Qiang Shao^{1, 4, a)}

¹⁾*Center for Quantum Sciences and School of Physics, Northeast Normal University, Changchun, 130024, China*

²⁾*Sino-European Institute of Aviation Engineering, Civil Aviation University of China, Tianjin 300300, China*

³⁾*Institute of High Performance Computing, A*STAR (Agency for Science, Technology and Research), 1 Fusionopolis Way, Connexis, Singapore 138632*

⁴⁾*Center for Advanced Optoelectronic Functional Materials Research, and Key Laboratory for UV Light-Emitting Materials and Technology of Ministry of Education, Northeast Normal University, Changchun 130024, China*

(Dated: 19 July 2024)

Laser-induced gauge fields in neutral atoms serve as a means of mimicking the effects of a magnetic field, providing researchers with a platform to explore behaviors analogous to those observed in condensed matter systems under real magnetic fields. Here, we propose a method to generate chiral motion in atomic excitations within the neutral atomic ground-state manifolds. This is achieved through the application of polychromatic driving fields coupled to the ground-Rydberg transition, along with unconventional Rydberg pumping. The scheme offers the advantage of arbitrary adjustment of the effective magnetic flux by setting the relative phases between different external laser fields. Additionally, the effective interaction strength between the atomic ground states can be maintained at 10 kHz, surpassing the capabilities of the previous approach utilizing Floquet modulation. Notably, the proposed method can be readily extended to implement a hexagonal neutral atom lattice, serving as the fundamental unit in realizing the Haldane model.

I. INTRODUCTION

Quantum simulation refers to the use of a controllable quantum system to model and understand the behavior of another quantum system that may be difficult to study directly.¹⁻⁹ A key objective of this approach is to explore exotic phases arising from nontrivial topology in quantum lattice models, such as topological insulators (TIs).¹⁰⁻¹³ These insulators showcase distinctive phases of matter, including the quantum Hall effect (QHE),^{14,15} and offer insight into the intrinsic properties of band structures. This methodology facilitates the integration of gauge fields into diverse physical systems,¹⁶⁻¹⁹ enabling the induction of chiral motion in atomic excitations. In earlier work, the transfer of chiral Fock states in the QED architecture of circuits was achieved.²⁰ Subsequently, superconducting qubits²¹⁻²⁵ and ultracold atom-based platforms²⁶⁻²⁸ became the widely used simulation platforms in the artificial gauge field. Recently, cavity-magnonics system²⁹ and chiral quantum spin liquids³⁰⁻³² had also been proposed to study these issues.

Compared with the above systems, neutral-atom systems with Rydberg interactions are considered a promising choice.³³⁻³⁹ The strong and controllable interactions of Rydberg atoms offer significant advantages in simulating various many-body problems, particularly in exploring exotic phases and dynamics. For example, topological bands and Chern insulators have been implemented in Rydberg atoms,⁴⁰⁻⁴³ the Peierls phase has been realized in Rydberg systems with exchange interactions,^{44,45} and gauge fields have been synthe-

sized in Rydberg-atom arrays.⁴⁶⁻⁴⁸ We note that the schemes mentioned above, utilizing neutral atoms for simulation, can encode either the qubit into a dipole-dipole coupled Rydberg states or the ground state and Rydberg state of the atom. However, it is essential to acknowledge that Rydberg states have a finite lifetime because of spontaneous emission, leading to decay into low-lying excited states, and blackbody radiation transfers the atom to nearby Rydberg states. Additionally, electrons in the Rydberg state are more susceptible to external fields, introducing additional sources of decoherence.

Chiral excitation current has been achieved in different systems, exhibiting unique physical properties.^{21,23,49,50} Recently, some of us have proposed a scheme for quantum state transfer within the ground-state manifolds of neutral atoms.⁵¹ This scheme proves effective in simulating various single-body physics phenomena while simultaneously minimizing the impact of the Rydberg excited state. In an equilateral triangular structure, a chiral motion of excitation becomes observable through the periodic modulation of weak pulses. However, the scalability of this method for achieving quantum simulations with a larger number of atoms is limited. Furthermore, there is no guarantee of consistent periods for two chiral evolutions. In this work, we address this limitation by driving the atoms through the application of polychromatic fields,⁴⁷ combined with the unconventional Rydberg pumping.⁵²⁻⁵⁵ The induction of an effective magnetic flux arises from complex-valued hopping amplitudes between different atoms on the sites, leading to the Peierls phase. Consequently, we can adjust the Peierls phase arbitrarily by setting the relative phases between different external laser fields. This approach allows us to generate a gauge field in an equilateral triangle system composed of three atoms, thereby breaking the time-reversal symmetry (TRS). Compared to the approach in Ref. 51, we eliminate the need to periodically switch on

^{a)}Authors to whom correspondence should be addressed: you_jiabin@ihpc.a-star.edu.sg and shaoxq644@nenu.edu.cn

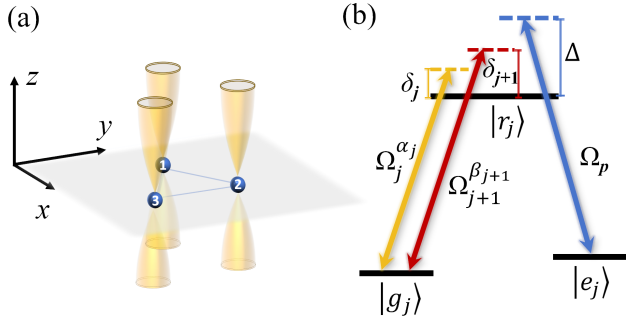


FIG. 1. (a) Three neutral atoms are arranged in an equilateral triangle in the $x-y$ plane. (b) The atomic structure in our scheme has three levels: $|g_j\rangle$, $|e_j\rangle$, and $|r_j\rangle$. Each atom is driven by one global laser field with real Rabi frequency Ω_p , detuned by Δ , and two local laser fields with complex Rabi frequencies $\Omega_j^{\alpha_j}$ and $\Omega_{j+1}^{\beta_{j+1}}$, detuned by δ_j and δ_{j+1} , respectively.

and off weak driving fields, enhancing the scalability of the present scheme.

II. REALIZATION OF CHIRAL MOTION IN THREE ATOMS

A. Model

The configuration of our setup is illustrated in Fig. 1(a), where three ^{87}Rb atoms form an equilateral triangle structure in the $x-y$ plane, maintaining uniform spacing R between each pair of atoms, and the quantization axis is z . In Fig. 1(b), the specific configuration of each atom is described, highlighting the ground states $|g\rangle = |5S_{1/2}, F=1, m_F=0\rangle$ and $|e\rangle = |5S_{1/2}, F=2, m_F=0\rangle$, in addition to the Rydberg state $|r\rangle = |60S_{1/2}, m_J=1/2\rangle$. The coupling between the ground state $|g\rangle$ of the j -th atom and the Rydberg state $|r\rangle$ involves two off-resonant local laser fields along the axis z which are characterized by complex Rabi frequencies $\Omega_j^{\alpha_j} = \Omega_j e^{i\alpha_j}$ and $\Omega_{j+1}^{\beta_{j+1}} = \Omega_{j+1} e^{i\beta_{j+1}}$ with positive real Ω_j ($j=1,2,3$), and the corresponding detunings are denoted by δ_j and δ_{j+1} , with the condition $\Omega_4^{\beta_4} = \Omega_1 e^{i\beta_1}$ and $\delta_4 = \delta_1$ for completeness. Additionally, the state $|e\rangle$ is coupled to $|r\rangle$ through a global laser field along the axis z , which is characterized by a real Rabi frequency Ω_p and is detuned by Δ . The van der Waals (vdW) interaction between Rydberg states takes the form of $\mathcal{U}_{i,j} = -C_6/R^6$, where the dispersion coefficient $C_6/(2\pi) \approx -135 \text{ GHz} \cdot \mu\text{m}^6$ ($\hbar=1$), as given by the second-order non-degenerate perturbation theory,⁵⁶ and R is the interatomic distance. Assuming $R \approx 2.96 \mu\text{m}$, we have $\mathcal{U}_{j,j+1}/(2\pi) = 200 \text{ MHz}$. Now, the full Hamiltonian of the

proposed model reads

$$H_I = \sum_{j=1}^3 [(\Omega_j^{\alpha_j} e^{-i\delta_j t} + \Omega_{j+1}^{\beta_{j+1}} e^{-i\delta_{j+1} t}) |r_j\rangle \langle g_j| + \Omega_p |r_j\rangle \langle e_j| e^{-i\Delta t} + \text{H.c.}] + \frac{1}{2} \sum_{i \neq j} \mathcal{U}_{i,j} |r_i r_j\rangle \langle r_i r_j|. \quad (1)$$

For simplicity, we assume that the Rydberg state directly decays into $|g\rangle$ and $|e\rangle$, with equal branching ratios for the spontaneous emission rates. This assumption establishes the subsequent consideration of independent decay channels $L_1 = \sqrt{\gamma/2} |g_1\rangle \langle r_1|$, $L_2 = \sqrt{\gamma/2} |e_1\rangle \langle r_1|$, $L_3 = \sqrt{\gamma/2} |g_2\rangle \langle r_2|$, $L_4 = \sqrt{\gamma/2} |e_2\rangle \langle r_2|$, $L_5 = \sqrt{\gamma/2} |g_3\rangle \langle r_3|$, and $L_6 = \sqrt{\gamma/2} |e_3\rangle \langle r_3|$. Therefore, the system's evolution is described by the Markovian master equation:

$$\dot{\rho} = -i[H_I, \rho] + \sum_{k=1}^6 L_k \rho L_k^\dagger - \frac{1}{2} \{L_k^\dagger L_k, \rho\}. \quad (2)$$

Now, we designate the state $|e\rangle$ in the ground-state manifold of neutral atoms as an effective “excited” state. Subsequently, we will elucidate the derivation process for the effective chiral dynamics of the dominant system within the single-“excitation” subspace $\{|egg\rangle, |geg\rangle, |gge\rangle\}$. When considering a rotating frame with respect to $U = \exp[-i \sum_{i \neq j} \mathcal{U}_{i,j}/2 |r_i r_j\rangle \langle r_i r_j| t]$, the high-frequency oscillation term can be disregarded due to the limit of large detuning $\mathcal{U}_{i,j} = \Delta \gg \{\Omega_p, \Omega_j, \delta_j\}$. As a result, the Hamiltonian of Eq. (1) can be reformulated as (see Appendix A for details):

$$H_I' = \sum_{j=1}^3 \Omega_j^{\alpha_j} \sigma_j^{rg} (P_{j+1}^e P_{j+2}^g + P_{j+1}^g P_{j+2}^e) e^{-i\delta_j t} + \Omega_{j+1}^{\beta_{j+1}} \sigma_j^{rg} (P_{j+1}^e P_{j+2}^g + P_{j+1}^g P_{j+2}^e) e^{-i\delta_{j+1} t} + \Omega_p \sigma_j^{re} (P_{j+1}^g P_{j+2}^r + P_{j+1}^r P_{j+2}^g) + \text{H.c.}, \quad (3)$$

with projection operator $P_j^k = |k_j\rangle \langle k_j|$ and transition operator $\sigma_j^{ab} = |a_j\rangle \langle b_j|$ (here $P_j^k = P_{j-3}^k$ and $\sigma_j^{ab} = \sigma_{j-3}^{ab}$ for $j > 3$). Eq. (3) can be transformed into a time-independent form by moving to another rotating frame defined by $U' = \exp\{-i[\delta_1(|egr\rangle \langle egr| + |rge\rangle \langle rge| + |rgr\rangle \langle rgr|)t + \delta_2(|erg\rangle \langle erg| + |reg\rangle \langle reg| + |rrg\rangle \langle rrg|)t + \delta_3(|ger\rangle \langle ger| + |gre\rangle \langle gre| + |grr\rangle \langle grr|)t]\}$. The resulting Hamiltonian is expressed as $H_I'' = H_0 + V_+ + V_+^\dagger$, where

$$H_0 = \Omega_p (|rgr\rangle \langle egr| + |rrg\rangle \langle erg| + |grr\rangle \langle ger| + |rrg\rangle \langle reg| + |rgr\rangle \langle rge| + |grr\rangle \langle gre|) + \text{H.c.} - \delta_1 (|egr\rangle \langle egr| + |rge\rangle \langle rge| + |rgr\rangle \langle rgr|) - \delta_2 (|erg\rangle \langle erg| + |reg\rangle \langle reg| + |rrg\rangle \langle rrg|) - \delta_3 (|ger\rangle \langle ger| + |gre\rangle \langle gre| + |grr\rangle \langle grr|), \quad (4)$$

which is essentially a block diagonalization matrix defined in three different subspaces $\{|egr\rangle, |rgr\rangle, |rge\rangle\}$, $\{|erg\rangle, |rrg\rangle, |reg\rangle\}$, and $\{|ger\rangle, |grr\rangle, |ger\rangle\}$, and $V_+ + V_+^\dagger$ can be regarded as a probe field for coupling the atomic ground

state to the single-excited Rydberg state, taking the form of

$$V_+ = \Omega_1^{\alpha_1} |rge\rangle \langle gge| + \Omega_2^{\beta_2} |reg\rangle \langle geg| + \Omega_2^{\alpha_2} |erg\rangle \langle egg| + \Omega_3^{\beta_3} |gre\rangle \langle gge| + \Omega_3^{\alpha_3} |ger\rangle \langle geg| + \Omega_1^{\beta_1} |egr\rangle \langle egg|. \quad (5)$$

Assuming $\{\Omega_p, |\delta_j|\} \gg \Omega_j$ and employing the effective operator formalism for open quantum systems,^{57–59} the effective Hamiltonian and the corresponding decay operators can be expressed by $H_{\text{eff}} = -\frac{1}{2}[V_+^\dagger H_0^{-1} V_+ + V_+^\dagger (H_0^{-1})^\dagger V_+]$ and $L_{\text{eff}}^k = L_k H_{NH}^{-1} V_+$, where $H_{NH} = H_0 - \frac{i}{2} \sum_j L_j^\dagger L_j$. Within the subspace of consideration, the concrete form of the effective coherent part reads

$$H_{\text{eff}} = \sum_{j=1}^3 J_{j,j+1} \sigma_j^- \sigma_{j+1}^+ + \text{H.c.}, \quad (6)$$

where

$$J_{j,j+1} = \frac{\Omega_{j+1}^{\alpha_{j+1}} (\Omega_{j+1}^{\beta_{j+1}})^* \Omega_p^2}{\delta_{j+1}^3 - 2\delta_{j+1} \Omega_p^2}, \quad (7)$$

which describes the effective coupling between ground-state atoms that carries a phase factor $e^{i\phi_{j,j+1}} = e^{i(\alpha_{j+1} - \beta_{j+1})}$ and the pseudo spin raising operator $\sigma_j^+ = |e_j\rangle \langle g_j|$. Note that in Eq. (6), the Stark-shift terms $[\Omega_1^2(\delta_1^2 - \Omega_p^2)/(\delta_1^3 - 2\delta_1 \Omega_p^2) + \Omega_2^2(\delta_2^2 - \Omega_p^2)/(\delta_2^3 - 2\delta_2 \Omega_p^2)]|egg\rangle \langle egg|$, $[\Omega_2^2(\delta_2^2 - \Omega_p^2)/(\delta_2^3 - 2\delta_2 \Omega_p^2) + \Omega_3^2(\delta_3^2 - \Omega_p^2)/(\delta_3^3 - 2\delta_3 \Omega_p^2)]|geg\rangle \langle geg|$, and $[\Omega_1^2(\delta_1^2 - \Omega_p^2)/(\delta_1^3 - 2\delta_1 \Omega_p^2) + \Omega_3^2(\delta_3^2 - \Omega_p^2)/(\delta_3^3 - 2\delta_3 \Omega_p^2)]|gge\rangle \langle gge|$ have been neglected since they can be easily canceled by introducing additional lasers. Correspondingly, the effective master equation is given by

$$\dot{\rho} = -i[H_{\text{eff}}, \rho] + \sum_{k=1}^6 L_{\text{eff}}^k \rho L_{\text{eff}}^{k\dagger} - \frac{1}{2} \{L_{\text{eff}}^{k\dagger} L_{\text{eff}}^k, \rho\}, \quad (8)$$

where the jump operators describing the dissipative part of the dynamics are $L_{\text{eff}}^1 = L_{1,1}^{(2)} + L_{3,3}^{(1)}$, $L_{\text{eff}}^2 = L_{2,1}^{(2)} + L_{4,3}^{(1)}$, $L_{\text{eff}}^3 = L_{3,1}^{(2)} + L_{1,2}^{(3)}$, $L_{\text{eff}}^4 = L_{4,1}^{(2)} + L_{2,2}^{(3)}$, $L_{\text{eff}}^5 = L_{3,2}^{(3)} + L_{1,3}^{(1)}$, and $L_{\text{eff}}^6 = L_{4,2}^{(3)} + L_{2,3}^{(1)}$, where

$$L_{1,j}^{(j)} = \Gamma_1^{(j)} |g_j e_{j+1}\rangle \langle g_j e_{j+1}| + \Gamma_2^{(j)} |g_j e_{j+1}\rangle \langle e_j g_{j+1}| + \Gamma_3^{(j)} (|g_j r_{j+1}\rangle \langle g_j e_{j+1}| + |g_j r_{j+1}\rangle \langle e_j g_{j+1}|), \quad (9)$$

$$L_{2,j}^{(j)} = \Gamma_1^{(j)} |e_j e_{j+1}\rangle \langle g_j e_{j+1}| + \Gamma_2^{(j)} |e_j e_{j+1}\rangle \langle e_j g_{j+1}| + \Gamma_3^{(j)} (|e_j r_{j+1}\rangle \langle g_j e_{j+1}| + |e_j r_{j+1}\rangle \langle e_j g_{j+1}|), \quad (10)$$

$$L_{3,j}^{(j)} = \Gamma_1^{(j)} |e_j g_{j+1}\rangle \langle e_j g_{j+1}| + \Gamma_2^{(j)} |e_j g_{j+1}\rangle \langle g_j e_{j+1}| + \Gamma_3^{(j)} (|r_j g_{j+1}\rangle \langle g_j e_{j+1}| + |r_j g_{j+1}\rangle \langle e_j g_{j+1}|), \quad (11)$$

$$L_{4,j}^{(j)} = \Gamma_1^{(j)} |e_j e_{j+1}\rangle \langle e_j g_{j+1}| + \Gamma_2^{(j)} |e_j e_{j+1}\rangle \langle g_j e_{j+1}| + \Gamma_3^{(j)} (|r_j e_{j+1}\rangle \langle g_j e_{j+1}| + |r_j e_{j+1}\rangle \langle e_j g_{j+1}|), \quad (12)$$

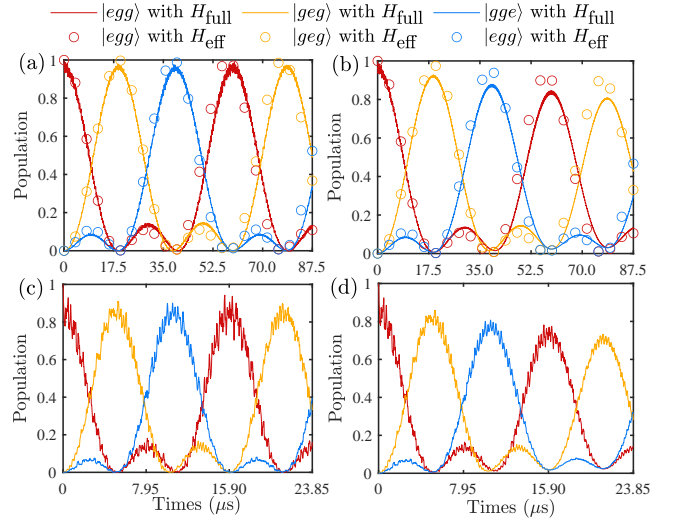


FIG. 2. The chiral motion of atomic excitation among the three atoms. (a) and (b) show chiral motion in the clockwise direction of the atoms, and the solid line represents the simulation carried out using the full master equation of Eq. (2), and the scatter denotes the simulation based on the effective master equation of Eq. (8). The parameters are $(\Omega_1, \Omega_2, \Omega_3, \Omega_p)/(2\pi) = (0.2, 0.2, 0.4, 4)$ MHz, $(\alpha_1, \alpha_{j \neq 1}, \beta_j) = (\pi/2, 0, 0)$, $(\delta_1, \delta_2, \delta_3, \Delta)/(2\pi) = (-4, 4, 8, 200)$ MHz, $\gamma/(2\pi) = 6.92$ kHz. (c) and (d) show population oscillations in a clockwise direction as governed by the master equation without and considering atomic decay. The parameters are changed to $(\Omega_1, \Omega_2, \Omega_3, \Omega_p)/(2\pi) = (0.4, 0.4, 0.8, 4)$ MHz, $(\alpha_1, \alpha_{j \neq 1}, \beta_j) = (\pi/2, 0, 0)$, $(\delta_1, \delta_2, \delta_3, \Delta)/(2\pi) = (-4, 4, 8, 200)$ MHz, $\gamma/(2\pi) = 6.92$ kHz.

with the effective spontaneous emission rates $\Gamma_1^{(j)} = |\Omega_j \chi (\gamma^2 - 3i\gamma\delta_j - 2\delta_j^2 + 2\Omega_p^2)/(\gamma - 2i\delta_j)|$, $\Gamma_2^{(j)} = |2\Omega_j \Omega_p^2 \chi / (\gamma - 2i\delta_j)|$, and $\Gamma_3^{(j)} = |(\Omega_j^{\alpha_j} + \Omega_j^{\beta_j}) \Omega_p \chi / 2|$, where $\chi = \sqrt{2\gamma}/(\gamma^2 - 3i\gamma\delta_j - 2\delta_j^2 + 4\Omega_p^2)$.

B. Numerical simulations

To ensure the generation of the ideal chiral motion of excitation, it is necessary to satisfy the following conditions: $|J_{12}| = |J_{23}| = |J_{31}|$ and synthetic flux $\Phi = (\alpha_2 - \beta_2) + (\alpha_3 - \beta_3) + (\alpha_1 - \beta_1) = \pm\pi/2$. For $\Phi = \pi/2$, the atomic excitation $|e\rangle$ propagates in the clockwise direction $1 \rightarrow 2 \rightarrow 3 \rightarrow 1$, and for $\Phi = -\pi/2$, the direction reverses, which breaks the TRS by the chiral motion of the system. In Figs. 2(a) and 2(b), we depict the population oscillations of states $|egg\rangle$, $|geg\rangle$, and $|gge\rangle$ versus the evolution time, starting from the state $|egg\rangle$. Under the parameters $\Omega_1 = \Omega_2 = 2\pi \times 0.2$ MHz, $\Omega_3 = 2\pi \times 0.4$ MHz, $\Omega_p = 2\pi \times 4$ MHz, $\delta_1 = -\delta_2 = 2\pi \times 4$ MHz, $\delta_3 = 2\pi \times 8$ MHz, we have the hopping strengths between the single-“excitation” states as $|J_{12}| = |J_{23}| = |J_{31}| = 2\pi \times 10$ kHz, which far exceed the coupling strength $J_{\text{eff}} = 2\pi \times 0.25$ (0.50) kHz utilizing Floquet modulation.⁵¹ We also choose $(\alpha_1, \alpha_{j \neq 1}, \beta_j) = (\pi/2, 0, 0)$ to ensure $\Phi = \pi/2$ to make the clockwise chiral motion of atomic excitation. The solid

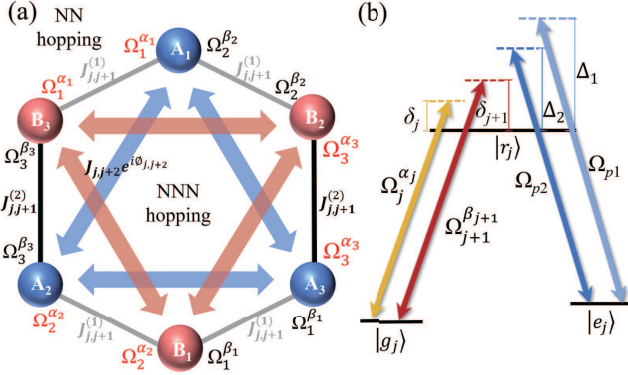


FIG. 3. (a) The hexagonal neutral atom lattice, and the specific solution for applying local laser fields to achieve the basis unit of the Haldane model. (b) The laser-atom interaction models.

line represents the simulation carried out using the full master equation of Eq. (2), while the scatter denotes the simulation based on the effective master equation of Eq. (8). The aforementioned findings show that the evolution under the effective master equation is fundamentally consistent with the full master equation. This observation suggests that each atom can be accurately described within a two-level subspace in accordance with our proposed scheme.

In fact, we can further strengthen the flip-flop interaction between ground states by adjusting the parameters without striving for perfect matching between the effective master equation and the full master equation. To reduce the period of population oscillation of chiral excitation, we set the parameters to $\Omega_1 = \Omega_2 = 2\pi \times 0.4$ MHz, $\Omega_3 = 2\pi \times 0.8$ MHz, $\Omega_p = 2\pi \times 4$ MHz, $\delta_1 = -\delta_2 = 2\pi \times 4$ MHz, $\delta_3 = 2\pi \times 8$ MHz, $\Delta = 2\pi \times 200$ MHz and $\gamma = 2\pi \times 6.92$ kHz. Figs. 2(c) and 2(d) illustrate the clockwise chiral motion of atomic excitation under the parameters $(\alpha_1, \alpha_{j \neq 1}, \beta_j) = (\pi/2, 0, 0)$, governed by the master equation without and with atomic decay, respectively. However, the system becomes more sensitive to spontaneous emission in this case due to the weaker suppression of Rydberg excitation. Therefore, although the effective hopping strength shown in Figs. 2(a) and 2(b) is relatively small, it allows for a longer coherence time in the system.

As shown in Eq. (7), the synthetic flux can be adjusted by varying the phases α_j and β_j of polychromatic driving fields, and the coupling strength depends solely on the Rabi frequency and detuning of the laser fields. Thus, this flexibility allows the scheme to be extended to a larger number of particles, allowing the simulation of more complex physical systems, such as the 2D triangular array.⁴⁶

III. HONEYCOMB LATTICE MODEL

The QHE has led to the discovery of a new type of material, TIs. In 1988, the first TI model, the Haldane model, was proposed,¹⁰ which revealed that the QHE can exhibit inherent properties of band structures rather than being caused by external magnetic fields. The Haldane model is a honeycomb

tight-binding lattice based on breaking both inversion symmetry (IS) and TRS. The exotic phases that arise from this model are considered to be at the forefront of condensed matter physics. Within a single cell of the honeycomb lattice, the difference in energy between two sublattices may disrupt the IS, and the complex next-nearest-neighbor (NNN) tunnel coupling can lead to the disruption of TRS. Furthermore, the total synthetic magnetic flux amounts to zero, thereby preserving the translational symmetry of the lattice.

The above-mentioned method for achieving chiral motion of excitation can be used directly to create a hexagonal neutral atom lattice, as shown in Fig. 3(a), with two separate sublattices, A and B, which break the IS. The quantization axis is perpendicular to the plane of the atoms. The distance between nearest-neighbor (NN) atoms is denoted as $R_{j,j+1}$, while the distance between NNN atoms is given by $R_{j,j+2} = \sqrt{3}R_{j,j+1}$. We apply two global driving fields with Rabi frequencies Ω_{p1} and Ω_{p2} that correspond to detunings Δ_1 and Δ_2 , respectively. The interaction between the NN atoms is denoted as $\mathcal{U}_{j,j+1} = \Delta_1$, and the interaction between NNN atoms is given by $\mathcal{U}_{j,j+2} = \Delta_2 = \Delta_1/(\sqrt{3})^6$, as illustrated in Fig. 3(b). Additionally, for the three atoms of sublattice A, laser fields $(\Omega_1^{\alpha_1}, \Omega_2^{\beta_2}), (\Omega_2^{\alpha_2}, \Omega_3^{\beta_3})$, and $(\Omega_3^{\alpha_3}, \Omega_1^{\beta_1})$ are applied to the atoms at points A_1, A_2 , and A_3 , respectively. Similarly, laser fields are applied to lattice points B_1, B_2 , and B_3 with pairs $(\Omega_1^{\beta_1}, \Omega_2^{\alpha_2}), (\Omega_2^{\beta_2}, \Omega_3^{\alpha_3})$, and $(\Omega_3^{\beta_3}, \Omega_1^{\alpha_1})$. All laser fields propagate along the quantization axis. This arrangement ensures that NN hopping occurs with the same phase α_j (β_j), while NNN hopping involves a phase difference of $\alpha_j - \beta_j$. As a result, a synthetic magnetic flux of $\pi/2$ is generated between triangles formed by each three-atom sublattice. In typical honeycomb tight-binding lattice models, a threefold rotational symmetry \mathcal{C}_3 exists due to identical NN and identical NNN hopping strengths. However, this symmetry can be broken and an extended model is obtained by introducing unequal NN hopping strengths, such as $J_{j,j+1}^{(1)} < J_{j,j+1}^{(2)}$, as discussed in Ref. 60. To simulate this model, we can choose specific parameters as follows: $\Omega_1 = \Omega_2 = 2\pi \times 0.03$ MHz, $\Omega_3 = 2\pi \times 0.0373$ MHz, $\Omega_{p1} = 2\pi \times 0.95$ MHz, $\Omega_{p2} = 2\pi \times 2.9$ MHz, $\delta_1 = -\delta_2 = 2\pi \times 1$ MHz, $\delta_3 = 2\pi \times 1.8$ MHz, $\Delta_1 = 2\pi \times 540$ MHz, and $\Delta_2 = 2\pi \times 20$ MHz. Therefore, we obtain $J_{j,j+1}^{(1)} = 2\pi \times 1$ kHz, $J_{j,j+1}^{(2)} = 2\pi \times 0.48588$ kHz, and $J_{j,j+2} = 2\pi \times 0.47845$ kHz.

IV. DISCUSSION

A. Experimental parameters

Now, we provide a concise discussion of the experimental feasibility of the proposed scheme. The transition from the ground states $|g\rangle$ or $|e\rangle$ to the Rydberg state $|r\rangle$ is facilitated through two-photon processes, as shown in Fig. 4. Specifically, the ground state $|g\rangle$ undergoes coupling to the intermediate state $|5P_{3/2}, F=1, m_F=-1\rangle$ using a local 780-nm σ^- polarized light. Subsequently, it is linked to $|r\rangle$ with another local 480-nm σ^+ polarized light. On the other hand,

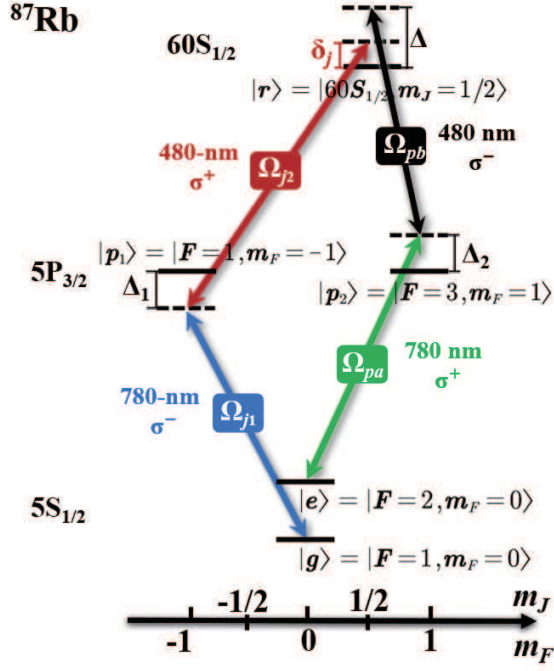


FIG. 4. Level structure for the proposed atomic system in ^{87}Rb and the laser-atom interaction model.

the alternate ground state $|e\rangle$ experiences excitation through a 780-nm σ^+ polarized light to reach the intermediate state $|p_2\rangle = |5P_{3/2}, F=3, m_F=1\rangle$, and subsequently, it connects to the Rydberg state $|r\rangle$ with a 480-nm σ^- polarized laser field. Given that the energy level difference between the two clock states $|g\rangle$ and $|e\rangle$ is $2\pi \times 6.83$ GHz, this substantial energy gap, in conjunction with the polarization of the optical fields, effectively suppresses excitation through alternative pathways. Additionally, recent experiments demonstrate that atoms can be cooled close to their motional ground state.⁶¹ By utilizing counterpropagating lasers with distinct polarizations, the impact of the Doppler effect is further mitigated. Furthermore, because all laser fields propagate along the z axis, the undesired relative phase between atoms caused by the laser can be neglected.

The configuration of each atom can be simplified to a three-level structure, as shown in Fig. 1(b), by adiabatically eliminating the intermediate states $|p_{1(2)}\rangle$. This simplification is achieved under the conditions $(\Omega_{j1}\Omega_{j2})/(4\Delta_1) = \Omega_j$ and $(\Omega_{pa}\Omega_{pb})/(4\Delta_2) = \Omega_p$, which require $\Omega_{j1}/(2\pi) = \Omega_{j2}/(2\pi) \approx 40\text{--}80$ MHz, $\Omega_{pa}/(2\pi) = \Omega_{pb}/(2\pi) \approx 179.5$ MHz, and $\Delta_1/(2\pi) = \Delta_2/(2\pi) \approx 2$ GHz. Specifically, $\Omega_{j1}/(2\pi) \approx 40\text{--}80$ MHz corresponds to a beam power P_{j1} of 12.31–49.26 nW and a waist of $1.5\text{ }\mu\text{m}$, while $\Omega_{j2}/(2\pi) \approx 40\text{--}80$ MHz corresponds to a beam power P_{j2} of 9.42–37.71 mW and a waist of $1.5\text{ }\mu\text{m}$. Similarly, $\Omega_{pa}/(2\pi) \approx 179.5$ MHz corresponds to a beam power P_{pa} of 11.48 μW and a waist of $10\text{ }\mu\text{m}$, and $\Omega_{pb}/(2\pi) \approx 179.5$ MHz corresponds to a beam power P_{pb} of 899.67 mW and a waist of $4\text{ }\mu\text{m}$.

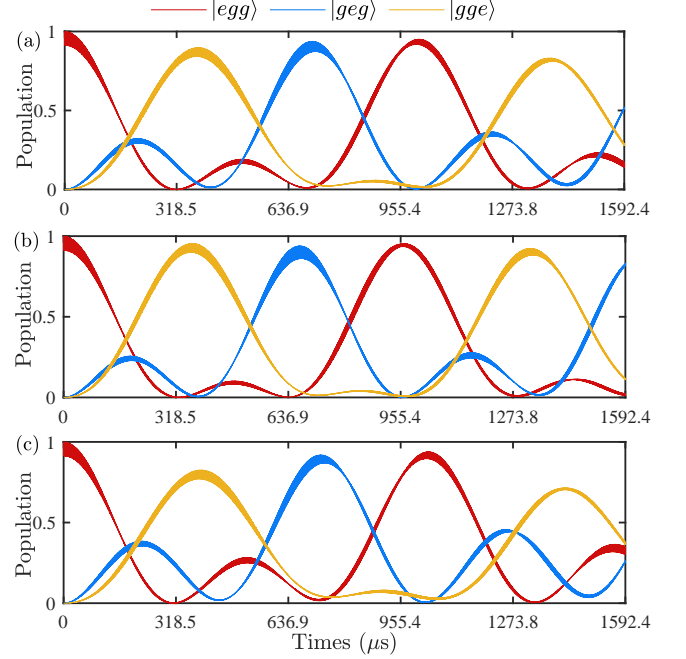


FIG. 5. Population oscillations of three-atom states $|gee\rangle$, $|ege\rangle$ and $|egg\rangle$. (a) $r_1 \approx 4.3447\text{ }\mu\text{m}$ with $\mathcal{U}_{j,j+2} = 2\pi \times 20$ MHz = Δ_2 . (b) $r_2 \approx 4.3647\text{ }\mu\text{m}$ with $\mathcal{U}_{j,j+2} = 2\pi \times 19.456$ MHz. (c) $r_3 \approx 4.3247\text{ }\mu\text{m}$ with $\mathcal{U}_{j,j+2} = 2\pi \times 20.561$ MHz. The parameters are $(\Omega_1, \Omega_2, \Omega_3, \Omega_p)/(2\pi) = (0.03, 0.03, 0.0373, 2.9)$ MHz, $(\delta_1, \delta_2, \delta_3, \Delta_2)/(2\pi) = (1, -1, 1.8, 20)$ MHz.

B. Undesired interatomic distance

In the preceding sections, we exclusively focused on the system characterized by the desired interatomic distance, where the Rydberg interaction strength equates to the corresponding blue-detuning parameter of the two-photon transition. However, it is essential to acknowledge that atoms exhibit positional fluctuations attributable to the finite temperature of traps and the repulsion induced by the vdW force. The incorporation of these position fluctuations for simulating multiple random quantum state evolution trajectories and subsequent averaging undoubtedly entails a significantly time-intensive process. To qualitatively explore the impact of imperfect atomic spacing, we adopt a fixed but undesired interatomic distance uniformly altered within the equilateral triangle structure depicted in Fig. 3(a), composed of $A_1 - A_2 - A_3$ or $B_1 - B_2 - B_3$. In Fig. 5(a), we plot the population oscillations of the three-atom states $|gee\rangle$, $|ege\rangle$, and $|egg\rangle$ at the desired interatomic distance $r_1 \approx 4.3447\text{ }\mu\text{m}$, satisfying $\Delta_2 = \mathcal{U}_{j,j+2} = 2\pi \times 20$ MHz. Figs. 5(b) and 5(c) illustrate the corresponding outcomes for $r_1 \pm 0.02\text{ }\mu\text{m}$, respectively. Evidently, within the considered range of atomic spacing, the periods of quantum state population evolution remain essentially consistent across all three cases, indicating no discernible dephasing effects. Nonetheless, this finding also underscores the necessity for stricter temperature control within the trap.

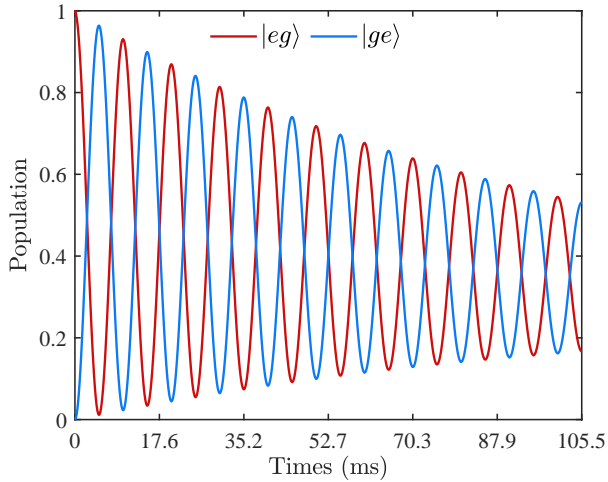


FIG. 6. Rabi oscillations of two atoms states $|eg\rangle$ and $|ge\rangle$ dominated by the master equation of Eq. (13).

C. Coherence time of the system

The Rabi oscillations between any pair of two atoms can be used to directly measure the coherence time of our model. As an example, we consider the dynamics of atoms A_1 and A_2 in Fig. 3(a). The effective flip-flop coupling strength between them is $2\pi \times 0.47845$ kHz, which corresponds to the full Hamiltonian of Eq. (1) with parameters $(\Omega_2, \Omega_p, \delta_2, \Delta)/(2\pi) = (0.0373, 2.9, 1, 20)$ MHz, as given by Sec. III. Specifically, the evolution of the system is governed by the Markovian master equation

$$\partial_t \rho = -i [H_I^{(2)}, \rho] + \sum_{j=1}^6 L_j \rho L_j^\dagger - \frac{1}{2} \{L_j^\dagger L_j, \rho\}, \quad (13)$$

where the Hamiltonian of the two atoms reads

$$\begin{aligned} H_I^{(2)} = & \Omega_2^\beta e^{-i\delta_2 t} |r_1\rangle\langle g_1| + \Omega_2^\alpha e^{-i\delta_2 t} |r_2\rangle\langle g_2| \\ & + \Omega_p \sum_{j=2}^3 |r_j\rangle\langle e_j| e^{-i\Delta t} + \text{H.c.} + \mathcal{U}_{1,2} |r_1 r_2\rangle\langle r_1 r_2|, \end{aligned} \quad (14)$$

and $L_1 = \sqrt{\gamma_1/2} |g_1\rangle\langle r_1|$, $L_2 = \sqrt{\gamma_1/2} |e_1\rangle\langle r_1|$, $L_3 = \sqrt{\gamma_1/2} |g_2\rangle\langle r_2|$, and $L_4 = \sqrt{\gamma_1/2} |e_2\rangle\langle r_2|$ with $\gamma_1/(2\pi) = 6.92$ kHz characterize the spontaneous emission of the Rydberg states to the computational basis states. Additionally, we have included the dephasing operators $L_5 = \sqrt{\gamma_2/2} |r_1\rangle\langle r_1|$ and $L_6 = \sqrt{\gamma_2/2} |r_2\rangle\langle r_2|$, where $\gamma_2/(2\pi) = 20$ kHz, to account for laser phase noise and other noise sources,^{62,63} for the sake of simplicity. We depict the population oscillations of states $|eg\rangle$ and $|ge\rangle$ versus the evolution time in Fig. 6. It can be observed that the $1/e$ coherence time of the system is 105.5 ms, which corresponds to 11.5 Rabi oscillations.

V. SUMMARY

In summary, by leveraging multi-color driving fields and an unconventional Rydberg pumping mechanism, we have developed a theoretical framework for achieving chiral motion of excitation in a three-atom system. This scheme offers highly adjustable parameters and successfully eliminates the previous reliance on modulation periods, as seen in conventional Floquet methods. Consequently, its applicability can be readily extended to multi-particle systems, such as the 2D triangular array and the honeycomb lattice. We also discussed the details of our proposed scheme, including the specific experimental setup and corresponding parameters. We found that imperfect atomic spacing does not significantly affect the period of population evolution, with no discernible dephasing effects. Additionally, we examined the coherence time of our model by considering the Rabi oscillations between any pair of two atoms. Compared to previously proposed schemes involving Rydberg atoms, we encode quantum information in the ground-state manifolds of neutral atoms and employ dispersion coupling between lasers and atoms, effectively minimizing spontaneous emission and mitigating the adverse effects of Rydberg state excitation. With these advancements, we anticipate that our proposed scheme can be experimentally implemented in the near future.

This work was supported by the National Natural Science Foundation of China (NSFC) under Grant No. 12174048, the Fundamental Research Funds for the Central Universities under Grant No. 3122023QD26, and the National Research Foundation Singapore (NRF2021-QEP2-02-P01), A*STAR Career Development Award (C210112010), and A*STAR (C230917003, C230917007).

AUTHOR DECLARATIONS

Conflict of Interest

The authors have no conflicts to disclose.

Author Contributions

Hao-Yuan Tang: Data curation (equal); Writing-original draft (lead). **Xiao-Xuan Li:** Data curation (equal). **Jia-Bin You:** Writing-review & editing (equal); Supervision (equal); Funding acquisition (equal). **Xiao-Qiang Shao:** Conceptualization (lead); Writing-review & editing (equal); Supervision (equal); Funding acquisition (equal).

DATA AVAILABILITY

The data that support the findings of this study are available from the corresponding authors upon reasonable request.

Appendix A: The details of Hamiltonian (3)

The full Hamiltonian of the equilateral triangle structure shown in Fig. 1(a) reads

$$\begin{aligned}
 H_I = & (\Omega_1^{\alpha_1} e^{-i\delta_1 t} + \Omega_2^{\beta_2} e^{-i\delta_2 t})|r_1\rangle\langle g_1| + (\Omega_2^{\alpha_2} e^{-i\delta_2 t} \\
 & + \Omega_3^{\beta_3} e^{-i\delta_3 t})|r_2\rangle\langle g_2| + (\Omega_3^{\alpha_3} e^{-i\delta_3 t} + \Omega_1^{\beta_1} e^{-i\delta_1 t})|r_3\rangle\langle g_3| \\
 & + \Omega_p \sum_{j=1}^3 |r_j\rangle\langle e_j| e^{-i\Delta t} + \text{H.c.} + \frac{1}{2} \sum_{i \neq j} \mathcal{U}_{i,j} |r_i r_j\rangle\langle r_i r_j|.
 \end{aligned} \quad (\text{A1})$$

Considering a rotating frame with respect to $U = \exp[-i \sum_{i \neq j} \mathcal{U}_{i,j}/2 |r_i r_j\rangle\langle r_i r_j| t]$, and $\mathcal{U}_{i,j} = \Delta$. The Hamiltonian satisfies $H_I' = iU^\dagger U + U^\dagger H_I U$, then the Eq. (A1) can be reformulated as:

$$\begin{aligned}
 H_I' = & \sum_{j=1}^3 \Omega_j^{\alpha_j} \sum_{k,k'=g,e} \sigma_j^{rg} [P_{j+1}^k P_{j+2}^{k'} e^{-i\delta_j t} + (P_{j+1}^r P_{j+2}^k \\
 & + P_{j+1}^{k'} P_{j+2}^r) e^{i\phi_j t}] + \Omega_{j+1}^{\beta_{j+1}} \sum_{k,k'=g,e} \sigma_j^{rg} [P_{j+1}^k P_{j+2}^{k'} e^{-i\delta_{j+1} t} \\
 & + (P_{j+1}^r P_{j+2}^k + P_{j+1}^{k'} P_{j+2}^r) e^{i\phi_{j+1} t}] + (\Omega_j^{\alpha_j} \sigma_j^{rg} P_{j+1}^r P_{j+2}^r \\
 & + \Omega_j^{\beta_j} \sigma_j^{rg} P_{j+1}^r P_{j+2}^r) e^{i\theta_j t} + \Omega_p [\sum_{k=g,e} P_j^r (\sigma_{j+1}^{re} P_{j+2}^k \\
 & + P_{j+1}^k \sigma_{j+2}^{re}) + \sum_{k,k'=g,e} \sigma_j^{re} P_{j+1}^k P_{j+2}^{k'} e^{-i\Delta t} \\
 & + \sigma_j^{re} P_{j+1}^r P_{j+2}^r e^{i\Delta t}] + \text{H.c.},
 \end{aligned} \quad (\text{A2})$$

where $\phi_i = \Delta - \delta_i$ and $\theta_i = 2\Delta - \delta_i$. The high-frequency oscillation term can be disregarded due to the limit of large detuning $\Delta \gg \{\Omega_p, \Omega_j, \delta_j\}$, then the Eq. (A2) is reduced to

$$\begin{aligned}
 H_I' = & \sum_{j=1}^3 \Omega_j^{\alpha_j} \sum_{k,k'=g,e} \sigma_j^{rg} P_{j+1}^k P_{j+2}^{k'} e^{-i\delta_j t} \\
 & + \Omega_{j+1}^{\beta_{j+1}} \sum_{k,k'=g,e} \sigma_j^{rg} P_{j+1}^k P_{j+2}^{k'} e^{-i\delta_{j+1} t} + \Omega_j^{\alpha_j} \sigma_j^{rg} P_{j+1}^r P_{j+2}^r \\
 & + \Omega_p \sum_{k=g,e} P_j^r (\sigma_{j+1}^{re} P_{j+2}^k + P_{j+1}^k \sigma_{j+2}^{re}) + \text{H.c.}
 \end{aligned} \quad (\text{A3})$$

The dynamics of the system we are considering are defined within three different subspaces $\{|egr\rangle, |rgr\rangle, |rge\rangle\}$, $\{|erg\rangle, |rrg\rangle, |reg\rangle\}$, and $\{|gre\rangle, |grr\rangle, |ger\rangle\}$. Thus, Eq. (A3)

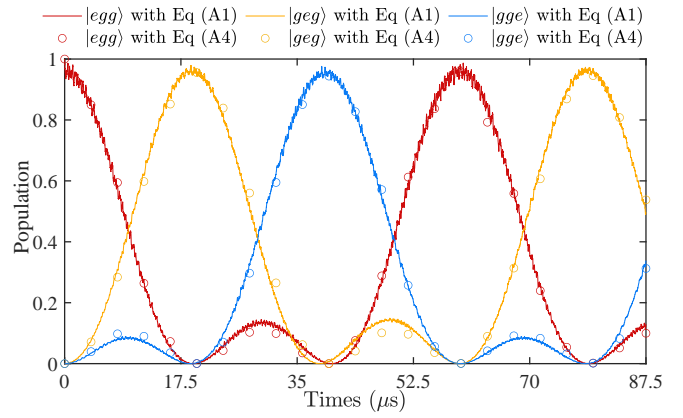


FIG. 7. The chiral motion of atomic excitation among the system governed by the full Hamiltonian (A1) and Eq. (A4), respectively. The parameters are $(\Omega_1, \Omega_2, \Omega_3, \Omega_p)/(2\pi) = (0.2, 0.2, 0.4, 4)$ MHz, $(\alpha_1, \alpha_{j \neq 1}, \beta_j) = (\pi/2, 0, 0)$, and $(\delta_1, \delta_2, \delta_3, \Delta)/(2\pi) = (-4, 4, 8, 200)$ MHz.

can be further rewritten as

$$\begin{aligned}
 H_I' = & \sum_{j=1}^3 \Omega_j^{\alpha_j} \sigma_j^{rg} (P_{j+1}^e P_{j+2}^g + P_{j+1}^g P_{j+2}^e) e^{-i\delta_j t} \\
 & + \Omega_{j+1}^{\beta_{j+1}} \sigma_j^{rg} (P_{j+1}^e P_{j+2}^g + P_{j+1}^g P_{j+2}^e) e^{-i\delta_{j+1} t} \\
 & + \Omega_p \sigma_j^{re} (P_{j+1}^g P_{j+2}^r + P_{j+1}^r P_{j+2}^g) + \text{H.c.}
 \end{aligned} \quad (\text{A4})$$

To verify the accuracy of our effective model, we compared the dynamics of the system governed by the full Hamiltonian (A1) with those described by Eq. (A4), as shown in Fig. 7. We found that these two cases match very well.

REFERENCES

- H. Bernien, S. Schwartz, A. Keesling, H. Levine, A. Omran, H. Pichler, S. Choi, A. S. Zibrov, M. Endres, M. Greiner, V. Vuletić, and M. D. Lukin, “Probing many-body dynamics on a 51-atom quantum simulator,” *Nature* **551**, 579–584 (2017).
- J. Zhang, G. Pagano, P. Hess, A. Kyprianidis, P. Becker, H. Kaplan, A. Gerskov, Z.-X. Gong, and C. Monroe, “Observation of a many-body dynamical phase transition with a 53-qubit quantum simulator,” *Nature* **551**, 601–604 (2017).
- S. Ebadi, T. T. Wang, H. Levine, A. Keesling, G. Semeghini, A. Omran, D. Bluvstein, R. Samajdar, H. Pichler, W. W. Ho, S. Choi, S. Sachdev, M. Greiner, V. Vuletić, and M. D. Lukin, “Quantum phases of matter on a 256-atom programmable quantum simulator,” *Nature* **595**, 227–232 (2021).
- J. Randall, C. Bradley, F. van der Gronden, A. Galicia, M. Abobeih, M. Markham, D. Twitchen, F. Machado, N. Yao, and T. Taminiau, “Many-body-localized discrete time crystal with a programmable spin-based quantum simulator,” *Science* **374**, 1474–1478 (2021).
- R. Babbush, J. McClean, D. Wecker, A. Aspuru-Guzik, and N. Wiebe, “Chemical basis of trotter-suzuki errors in quantum chemistry simulation,” *Phys. Rev. A* **91**, 022311 (2015).
- J. Argüello-Luengo, A. González-Tudela, T. Shi, P. Zoller, and J. I. Cirac, “Analogue quantum chemistry simulation,” *Nature* **574**, 215–218 (2019).
- R. D. Somma, C. D. Batista, and G. Ortiz, “Quantum approach to classical statistical mechanics,” *Phys. Rev. Lett.* **99**, 030603 (2007).

- ⁸H. B. Kaplan, L. Guo, W. L. Tan, A. De, F. Marquardt, G. Pagano, and C. Monroe, “Many-body dephasing in a trapped-ion quantum simulator,” *Phys. Rev. Lett.* **125**, 120605 (2020).
- ⁹J. Casanova, L. Lamata, I. L. Egusquiza, R. Gerritsma, C. F. Roos, J. J. García-Ripoll, and E. Solano, “Quantum simulation of quantum field theories in trapped ions,” *Phys. Rev. Lett.* **107**, 260501 (2011).
- ¹⁰F. D. M. Haldane, “Model for a quantum hall effect without landau levels: Condensed-matter realization of the “parity anomaly,”” *Phys. Rev. Lett.* **61**, 2015–2018 (1988).
- ¹¹M. Z. Hasan and C. L. Kane, “Colloquium: Topological insulators,” *Rev. Mod. Phys.* **82**, 3045–3067 (2010).
- ¹²G. Jotzu, M. Messer, R. Desbuquois, M. Lebrat, T. Uehlinger, D. Greif, and T. Esslinger, “Experimental realization of the topological haldane model with ultracold fermions,” *Nature* **515**, 237 – 240 (2014).
- ¹³D.-W. Wang, H. Cai, L. Yuan, S.-Y. Zhu, and R.-B. Liu, “Topological phase transitions in superradiance lattices,” *Optica* **2**, 712–715 (2015).
- ¹⁴K. v. Klitzing, G. Dorda, and M. Pepper, “New method for high-accuracy determination of the fine-structure constant based on quantized hall resistance,” *Phys. Rev. Lett.* **45**, 494–497 (1980).
- ¹⁵D. C. Tsui, H. L. Stormer, and A. C. Gossard, “Two-dimensional magnetotransport in the extreme quantum limit,” *Phys. Rev. Lett.* **48**, 1559–1562 (1982).
- ¹⁶M. Aidelsburger, M. Atala, S. Nascimbène, S. Trotzky, Y.-A. Chen, and I. Bloch, “Experimental realization of strong effective magnetic fields in an optical lattice,” *Phys. Rev. Lett.* **107**, 255301 (2011).
- ¹⁷A. R. Kolovsky, “Creating artificial magnetic fields for cold atoms by photon-assisted tunneling,” *Europhysics Letters* **93**, 20003 (2011).
- ¹⁸N. Goldman and J. Dalibard, “Periodically driven quantum systems: Effective hamiltonians and engineered gauge fields,” *Phys. Rev. X* **4**, 031027 (2014).
- ¹⁹M. Schmidt, S. Kessler, V. Peano, O. Painter, and F. Marquardt, “Optomechanical creation of magnetic fields for photons on a lattice,” *Optica* **2**, 635–641 (2015).
- ²⁰J. Koch, A. A. Houck, K. L. Hur, and S. M. Girvin, “Time-reversal-symmetry breaking in circuit-qed-based photon lattices,” *Phys. Rev. A* **82**, 043811 (2010).
- ²¹P. Roushan, C. Neill, A. Megrant, Y. Chen, R. Babbush, R. Barends, B. Campbell, Z. Chen, B. Chiaro, A. Dunsworth, *et al.*, “Chiral ground-state currents of interacting photons in a synthetic magnetic field,” *Nature Physics* **13**, 146–151 (2017).
- ²²D.-W. Wang, C. Song, W. Feng, H. Cai, D. Xu, H. Deng, H. Li, D. Zheng, X. Zhu, H. Wang, *et al.*, “Synthesis of antisymmetric spin exchange interaction and chiral spin clusters in superconducting circuits,” *Nature Physics* **15**, 382–386 (2019).
- ²³W. Liu, W. Feng, W. Ren, D.-W. Wang, and H. Wang, “Synthesizing three-body interaction of spin chirality with superconducting qubits,” *Applied Physics Letters* **116**, 114001 (2020).
- ²⁴X. Guan, Y. Feng, Z.-Y. Xue, G. Chen, and S. Jia, “Synthetic gauge field and chiral physics on two-leg superconducting circuits,” *Phys. Rev. A* **102**, 032610 (2020).
- ²⁵Y.-I. Ren, S.-I. Ma, and F.-I. Li, “Chiral coupling between a ferromagnetic magnon and a superconducting qubit,” *Phys. Rev. A* **106**, 053714 (2022).
- ²⁶J. Dalibard, F. Gerbier, G. Juzeliūnas, and P. Öhberg, “Colloquium: Artificial gauge potentials for neutral atoms,” *Rev. Mod. Phys.* **83**, 1523–1543 (2011).
- ²⁷M. Aidelsburger, S. Nascimbene, and N. Goldman, “Artificial gauge fields in materials and engineered systems,” *Comptes Rendus Physique* **19**, 394–432 (2018).
- ²⁸N. R. Cooper, J. Dalibard, and I. B. Spielman, “Topological bands for ultracold atoms,” *Rev. Mod. Phys.* **91**, 015005 (2019).
- ²⁹S.-F. Qi and J. Jing, “Chiral current in floquet cavity magnonics,” *Phys. Rev. A* **106**, 033711 (2022).
- ³⁰B. Bauer, L. Cincio, B. P. Keller, M. Dolfi, G. Vidal, S. Trebst, and A. W. Ludwig, “Chiral spin liquid and emergent anyons in a kagome lattice mott insulator,” *Nature communications* **5**, 5137 (2014).
- ³¹A. Ralko and J. Merino, “Novel chiral quantum spin liquids in kitaev magnets,” *Phys. Rev. Lett.* **124**, 217203 (2020).
- ³²P. S. Tarabunga, G. Giudici, T. Chanda, and M. Dalmonte, “Classification and emergence of quantum spin liquids in chiral rydberg models,” *Phys. Rev. B* **108**, 075118 (2023).
- ³³M. Saffman, T. G. Walker, and K. Mølmer, “Quantum information with rydberg atoms,” *Rev. Mod. Phys.* **82**, 2313–2363 (2010).
- ³⁴M. Saffman, “Quantum computing with atomic qubits and rydberg interactions: progress and challenges,” *Journal of Physics B: Atomic, Molecular and Optical Physics* **49**, 202001 (2016).
- ³⁵D. Barredo, S. De Léséleuc, V. Lienhard, T. Lahaye, and A. Browaeys, “An atom-by-atom assembler of defect-free arbitrary two-dimensional atomic arrays,” *Science* **354**, 1021–1023 (2016).
- ³⁶X. Wu, X. Liang, Y. Tian, F. Yang, C. Chen, Y.-C. Liu, M. K. Tey, and L. You, “A concise review of rydberg atom based quantum computation and quantum simulation,” *Chinese Physics B* **30**, 020305 (2021).
- ³⁷M. Morgado and S. Whitlock, “Quantum simulation and computing with rydberg-interacting qubits,” *AVS Quantum Science* **3** (2021).
- ³⁸X.-F. Shi, “Quantum logic and entanglement by neutral rydberg atoms: methods and fidelity,” *Quantum Science and Technology* **7**, 023002 (2022).
- ³⁹X.-Q. Shao, S.-L. Su, L. Li, R. Nath, J.-H. Wu, and W. Li, “Rydberg superatoms: An artificial quantum system for quantum information processing and quantum optics,” *arXiv preprint arXiv:2404.05330* (2024).
- ⁴⁰D. Peter, N. Y. Yao, N. Lang, S. D. Huber, M. D. Lukin, and H. P. Büchler, “Topological bands with a chern number $c = 2$ by dipolar exchange interactions,” *Phys. Rev. A* **91**, 053617 (2015).
- ⁴¹S. Weber, S. de Léséleuc, V. Lienhard, D. Barredo, T. Lahaye, A. Browaeys, and H. P. Büchler, “Topologically protected edge states in small rydberg systems,” *Quantum Science and Technology* **3**, 044001 (2018).
- ⁴²S. Weber, R. Bai, N. Makki, J. Mögerle, T. Lahaye, A. Browaeys, M. Daghofer, N. Lang, and H. P. Büchler, “Experimentally accessible scheme for a fractional chern insulator in rydberg atoms,” *PRX Quantum* **3**, 030302 (2022).
- ⁴³Y. Zhao and X.-F. Shi, “Fractional chern insulator with rydberg-dressed neutral atoms,” *Phys. Rev. A* **108**, 053107 (2023).
- ⁴⁴X.-F. Shi and T. A. B. Kennedy, “Simulating magnetic fields in rydberg-dressed neutral atoms,” *Phys. Rev. A* **97**, 033414 (2018).
- ⁴⁵V. Lienhard, P. Scholl, S. Weber, D. Barredo, S. de Léséleuc, R. Bai, N. Lang, M. Fleischhauer, H. P. Büchler, T. Lahaye, and A. Browaeys, “Realization of a density-dependent peierls phase in a synthetic, spin-orbit coupled rydberg system,” *Phys. Rev. X* **10**, 021031 (2020).
- ⁴⁶S. Ohler, M. Kiefer-Emmanouilidis, A. Browaeys, H. P. Büchler, and M. Fleischhauer, “Self-generated quantum gauge fields in arrays of rydberg atoms,” *New Journal of Physics* **24**, 023017 (2022).
- ⁴⁷X. Wu, F. Yang, S. Yang, K. Mølmer, T. Pohl, M. K. Tey, and L. You, “Manipulating synthetic gauge fluxes via multicolor dressing of rydberg-atom arrays,” *Phys. Rev. Res.* **4**, L032046 (2022).
- ⁴⁸N. E. Palaiodimopoulos, S. Ohler, M. Fleischhauer, and D. Petrosyan, “Chiral quantum router with rydberg atoms,” *Phys. Rev. A* **109**, 032622 (2024).
- ⁴⁹F.-H. Wang, X.-L. Lu, J.-J. Zou, and Z.-L. Xiang, “Chiral excitation flows of multinode network based on synthetic gauge fields,” *arXiv preprint arXiv:2312.02009* (2023).
- ⁵⁰S. Wang, W. Zhang, C. Sun, C. Wu, X. Shao, and G. Wang, “Ground-state chiral current via periodic modulation,” *arXiv preprint arXiv:2403.06688* (2024).
- ⁵¹X. X. Li, J. B. You, X. Q. Shao, and W. Li, “Coherent ground-state transport of neutral atoms,” *Phys. Rev. A* **105**, 032417 (2022).
- ⁵²D. X. Li and X. Q. Shao, “Unconventional rydberg pumping and applications in quantum information processing,” *Phys. Rev. A* **98**, 062338 (2018).
- ⁵³X.-Q. Shao, “Selective rydberg pumping via strong dipole blockade,” *Phys. Rev. A* **102**, 053118 (2020).
- ⁵⁴X. Q. Shao, F. Liu, X. W. Xue, W. L. Mu, and W. Li, “High-fidelity interconversion between greenberger-horne-zeilinger and w states through floquet-lindblad engineering in rydberg atom arrays,” *Phys. Rev. Appl.* **20**, 014014 (2023).
- ⁵⁵Y. Zhao, Y.-Q. Yang, W. Li, and X.-Q. Shao, “Dissipative stabilization of high-dimensional GHZ states for neutral atoms,” *Applied Physics Letters* **124**, 114001 (2024).
- ⁵⁶N. Šibalić, J. Pritchard, C. Adams, and K. Weatherill, “Arc: An open-source library for calculating properties of alkali rydberg atoms,” *Computer Physics Communications* **220**, 319–331 (2017).
- ⁵⁷M. J. Kastoryano, F. Reiter, and A. S. Sørensen, “Dissipative preparation of entanglement in optical cavities,” *Phys. Rev. Lett.* **106**, 090502 (2011).

- ⁵⁸F. Reiter and A. S. Sørensen, “Effective operator formalism for open quantum systems,” *Phys. Rev. A* **85**, 032111 (2012).
- ⁵⁹F. Reiter, L. Tornberg, G. Johansson, and A. S. Sørensen, “Steady-state entanglement of two superconducting qubits engineered by dissipation,” *Phys. Rev. A* **88**, 032317 (2013).
- ⁶⁰B. Wang, X. Zhou, H. Lin, and A. Bansil, “Higher-order topological insulator phase in a modified haldane model,” *Phys. Rev. B* **104**, L121108 (2021).
- ⁶¹Z. Tian, H. Chang, X. Lv, M. Yang, Z. Wang, P. Yang, P. Zhang, G. Li, and T. Zhang, “Resolved raman sideband cooling of a single optically trapped cesium atom,” *Opt. Lett.* **49**, 542–545 (2024).
- ⁶²W. Lee, M. Kim, H. Jo, Y. Song, and J. Ahn, “Coherent and dissipative dynamics of entangled few-body systems of rydberg atoms,” *Phys. Rev. A* **99**, 043404 (2019).
- ⁶³K. Kim, F. Yang, K. Mølmer, and J. Ahn, “Realization of an extremely anisotropic heisenberg magnet in rydberg atom arrays,” *Phys. Rev. X* **14**, 011025 (2024).